

The influence of bidirectional tidal flow on scour mechanisms and morphological changes around the Suramadu bridge piers

Zidny Omnu Nurilhaq¹, Candida Aulia De Silva Nusantara^{1*}, Khomsin¹, Danar Guruh Pratomo¹, and Irena Hana Hariyanto¹

¹Department of Geomatics Engineering, Faculty of Civil Planning and Geo Engineering, Institut Teknologi Sepuluh Nopember, Sukolilo, Surabaya 60111, Indonesia

*Corresponding author: candida.nusantara@its.ac.id

Abstract. The Suramadu Bridge is a vital infrastructure in the Madura Strait, facilitating regional economic connectivity. However, complex oceanographic characteristics—notably bidirectional currents and seasonal variations—pose significant scouring risks to bridge piers, potentially threatening structural integrity. This study models current patterns and sediment transport to analyze scouring dynamics around the piers. Using hydrodynamics model, simulations were conducted for 2024, incorporating bathymetry, tides, wind, and sediment data. Model validation against tidal data showed high accuracy (MAE: 0.1473 m; RMSE: 0.1771 m). Results reveal a tidal-driven west–east bidirectional flow with stable average velocities (0.21–0.25 m/s) across monsoons. Interaction between currents and piers causes upstream flow deceleration and lateral acceleration, triggering deposition and erosion, respectively. Piers P46, P47, and P49 experienced the most significant scouring, with maximum depths reaching -0.250 m, while P37, P41, and P56 remained stable. Erosion trends were spatially and temporally consistent across both west and east monsoons. These findings establish critical monitoring priorities to ensure the bridge’s structural sustainability in alignment with SDG Goal 9.

Keywords: current patterns, hydrodynamic modelling, scouring, sediment transport, sustainable infrastructure

1. Introduction

The Surabaya–Madura Bridge, widely known as the Suramadu Bridge, is the longest bridge in Indonesia with a total length of 5,438 meters. Its construction began under Presidential Decree No. 55 of 1990, later revised by Presidential Decree No. 79 of 2003, and was officially opened on 10 June 2009 [1]. The bridge connects Surabaya on Java Island with Bangkalan on Madura Island, crossing the Madura Strait. As the only direct land connection between Java and Madura, it plays a crucial role in enhancing regional connectivity and supporting socio-economic development. Since becoming operational, the bridge has significantly

improved mobility, facilitated the movement of goods and people, and contributed to the economic growth of the four regencies in Madura [2].

However, the location of the bridge within Madura Strait introduces considerable challenges. The strait exhibits complex oceanographic characteristics, including a bidirectional current system driven by tidal forcing and seasonal monsoonal patterns. During the west monsoon, the current flows from the Java Sea toward the Madura Strait, while during the east monsoon it reverses toward the Bali Sea [3]. Recorded current velocities range from 0.03 to 0.41 m/s [4], and when combined with varying sediment types such as sandy clay and silt, they contribute to potential seabed alterations around the bridge structure [5]. One of the most critical risks associated with these conditions is local scour, a localized erosion process around bridge foundations driven by flow-induced sediment entrainment. Its mechanisms often involve three-dimensional flow structures and horseshoe vortices forming at the base of piers [6]. If not properly mitigated, scouring can compromise foundation stability and lead to structural failure.

Several studies have attempted to model scouring phenomena at the Suramadu Bridge, including applications of HEC-18 and Hanco methods [7]. However, previous research relied on single-direction flow assumptions and lacked comprehensive seasonal integration [8]. Addressing these limitations, this study models current dynamics and sediment transport around the bridge piers by incorporating bidirectional tidal flow and seasonal variability through a year-long numerical hydrodynamic simulation. This approach provides a more complete understanding of scour behavior and supports resilient and sustainable infrastructure management strategies aligned with Sustainable Development Goal (SDG) 9.

2. Research method

2.1 Study area

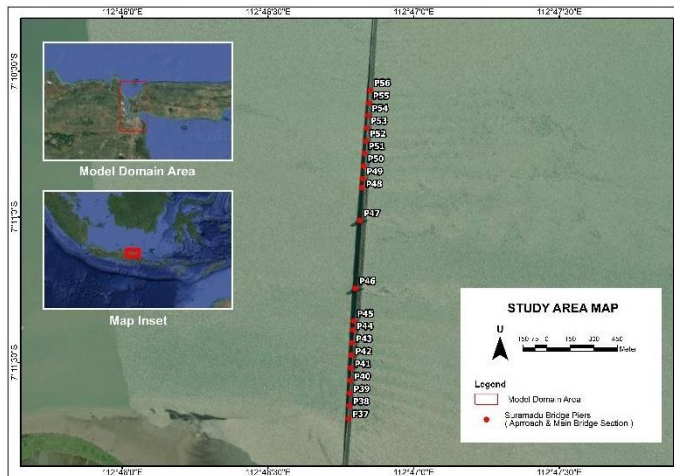


Fig. 1. Study location map in the Madura Strait waters.

The study area is located within the waters of the Madura Strait surrounding the Suramadu Bridge. The modeling domain encompasses the administrative marine boundaries of Surabaya City, Bangkalan Regency, and Gresik Regency, covering an area of approximately 1,514.63 km², as illustrated in Figure 1. The geographical extent of the study area ranges from 6°52'4.45" S to 7°20'40.36" S and from 112°36'10.40" E to 112°52'4.45" E. The focus of the scour analysis is highlighted by red markers indicating the coordinates of the Suramadu

Bridge piers, consisting of both the approach bridge and main bridge sections, with detailed information provided in Table 1.

Table 1. Coordinates of the Suramadu Bridge Piers (Approach and Main Bridge Sections)

Piers Number	Section	Latitude	Longitude
P37	<i>Approach Bridge</i>	-7°11'41.55"	112°46'46.60"
P38	<i>Approach Bridge</i>	-7°11'38.92"	112°46'46.71"
P39	<i>Approach Bridge</i>	-7°11'36.32"	112°46'46.83"
P40	<i>Approach Bridge</i>	-7°11'33.71"	112°46'46.95"
P41	<i>Approach Bridge</i>	-7°11'31.12"	112°46'47.06"
P42	<i>Approach Bridge</i>	-7°11'28.49"	112°46'47.18"
P43	<i>Approach Bridge</i>	-7°11'25.92"	112°46'47.32"
P44	<i>Approach Bridge</i>	-7°11'23.29"	112°46'47.46"
P45	<i>Approach Bridge</i>	-7°11'21.44"	112°46'47.57"
P46	<i>Main Bridge</i>	-7°11'14.72"	112°46'47.98"
P47	<i>Main Bridge</i>	-7°11'0.77"	112°46'48.91"
P48	<i>Approach Bridge</i>	-7°10'53.99"	112°46'49.38"
P49	<i>Approach Bridge</i>	-7°10'52.13"	112°46'49.51"
P50	<i>Approach Bridge</i>	-7°10'49.51"	112°46'49.72"
P51	<i>Approach Bridge</i>	-7°10'46.92"	112°46'49.92"
P52	<i>Approach Bridge</i>	-7°10'44.36"	112°46'50.15"
P53	<i>Approach Bridge</i>	-7°10'41.69"	112°46'50.38"
P54	<i>Approach Bridge</i>	-7°10'39.12"	112°46'50.60"
P55	<i>Approach Bridge</i>	-7°10'36.54"	112°46'50.82"
P56	<i>Approach Bridge</i>	-7°10'33.93"	112°46'51.05"

2.2 Data and equipment

This study utilized various instruments and software to support primary data acquisition, data processing, and hydrodynamic modelling. The equipment consisted of a Single Beam Echosounder (SBES) for obtaining bathymetric data around the Suramadu Bridge piers and a grab sampler for collecting sediment samples at six locations.

The datasets used in this research comprised model domain construction data, model input data, and model validation data. The model domain was developed using shoreline administrative data for East Java Province from the Geospatial Information Agency (BIG) and the pier dimension data obtained from CCCC Highway & Bridge Consultants Co., Ltd. [9]. Bathymetry data were sourced from direct field measurements carried out from 1–7 July 2024, global bathymetry from BATNAS, and digitized Indonesian nautical charts. The model input included tidal forcing for 2024, global wind data for 2024 derived from ERA5 reanalysis [10], and river discharge data from the Kalimas River obtained from previous studies [11]. Sediment characteristics were obtained from laboratory analyses of samples collected from 1–7 July 2024, while wave parameters were extracted from ERA5 [10] for sediment transport modelling. Model validation was conducted using tidal observations from the BIG tide gauge station SRBY for the year 2024.

2.3 Research workflow

The study began with the identification of key issues related to bridge pier scouring, followed by an extensive literature review on hydrodynamic modeling approaches and the relevant oceanographic parameters within the study area. Subsequently, both primary and secondary

datasets were collected and processed to support the development of the hydrodynamic and sediment transport models. These steps include domain construction, numerical model setup, calibration and validation, and analysis of current patterns, sediment transport, and scour formation.

2.3.1 Domain construction

The land boundary was defined by following the coastline derived from the Rupa Bumi Indonesia (RBI) shoreline dataset for East Java Province, covering the coastal areas of Surabaya City, Gresik Regency, and Bangkalan Regency. The open boundaries were assigned along the northern edge of the domain, with a length of approximately 23 km, and along the eastern edge, extending about 10 km. An additional boundary was applied at the Kalimas River, with the width set to 100 m to represent the river mouth.

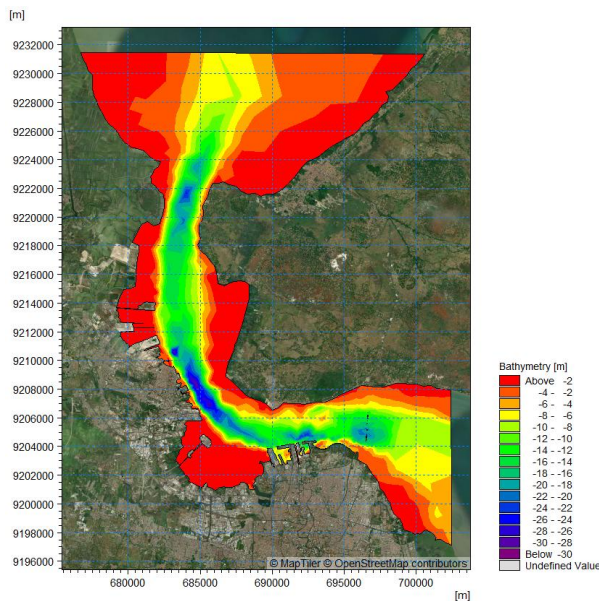


Fig. 2. Hydrodynamic model domain.

In constructing the model domain, an unstructured triangular grid (flexible mesh) was applied, combined with multiple bathymetric datasets. High-resolution depth data were obtained from direct field measurements using a Single Beam Echosounder (SBES) around the Suramadu Bridge piers to enhance detail within the focus area. These data were integrated with digitized Indonesian nautical charts and the National Bathymetry (BATNAS) dataset, which provided wider-area depth coverage referenced to Mean Sea Level (MSL). The resulting interpolated bathymetry, illustrated in **Fig. 2**, shows significant depth variability in the Madura Strait, ranging from shallow nearshore waters at 0 m to deeper sections along the main navigation channel reaching 30.445 m. This spatial depth distribution plays an essential role in influencing current patterns, sediment transport dynamics, and scouring processes around the bridge piers.

2.3.2 Numerical model setup

The hydrodynamic and sediment transport simulations were conducted using hydrodynamic model. Wind and wave input parameters were extracted using Ocean Data View prior to

being incorporated into the model. The extracted wind and wave datasets, along with tidal forcing, river discharge, and sediment grain size (D50), were then used as boundary and initial conditions for the hydrodynamic and sediment transport simulations. The model was run for a full one-year period, from January 2024 to December 2024. The temporal parameters used in the simulation are summarized in **Table 2**.

Table 2. Simulation time parameters

Parameter	Value
Simulation period	373 days
Simulation soft start	7 days
Start time	24 December 2023
Stop time	31 December 2024
Time step interval	1 second

The simulation was carried out over a total duration of 373 days, starting on 24 December 2023 and ending on 31 December 2024. A soft start period of 7 days was applied at the beginning of the simulation to gradually stabilize the model and prevent numerical shocks, ensuring a smooth transition toward realistic hydrodynamic conditions. This soft start phase is crucial for minimizing initial transients and improving the accuracy of the subsequent results. A time step interval of 1 second was selected due to the use of an unstructured grid, in which element sizes vary considerably across the model domain. A larger time step could violate numerical stability constraints and lead to unrealistic outputs or model instability. The chosen 1-second interval is sufficiently small to maintain the Courant number below critical thresholds while remaining computationally efficient for a year-long simulation.

2.3.3 Calibration and validation

Before analyzing the model results, a validation procedure was conducted to assess how well the model represents real-world conditions. This validation compared the simulated tidal water levels with observational tidal data recorded by the Geospatial Information Agency (BIG) at the Surabaya tide gauge station. Statistical performance was evaluated using the Mean Absolute Error (MAE) and Root Mean Square Error (RMSE) metrics. The formulations for MAE and RMSE are presented in **equations (1) and (2)** [12].

$$MAE = \frac{1}{N} \sum_{i=1}^N |OBS_i - SIM_i| \tag{1}$$

$$RMSE = \sqrt{\frac{1}{N} \sum_{i=1}^N (OBS_i - SIM_i)^2} \tag{2}$$

where N represents the number of data points (observations), OBS_i denotes the actual observational value, and SIM_i denotes the model-predicted value. The error categories for MAE and RMSE are presented in **Table 3**.

Table 3. Interpretation of MAE and RMSE value [12]

MAE and RMSE value	Error level
0 – 0.299	Small
0.30 – 0.599	Medium
0.60 – 0.899	Large
>0.90	Very large

2.3.4 Current pattern and sediment transport analysis

The current and sediment transport parameters serve as the basis for evaluating the scouring mechanism around the bridge piers. Current patterns were analyzed to identify the dominant hydrodynamic forces responsible for mobilizing seabed sediments and their interaction with the pier structures. Meanwhile, sediment transport patterns were examined to determine the spatial distribution of sediment movement and its response to the prevailing flow conditions. The analysis of current and sediment transport patterns was conducted for both the west and east monsoon seasons under spring and neap tide conditions, along with an assessment of current distribution and its interaction with the bridge piers.

2.3.5 Scouring analysis

The scouring analysis was carried out by examining the interaction between current patterns and sediment transport around the bridge piers, which leads to the development of local scour at the Suramadu Bridge. The scouring assessment involved comparing the cumulative erosion values observed during the west and east monsoon seasons around each pier. This analysis was further extended by calculating the annual scour depth and scour rate using a linear regression approach, as formulated in **equation (3)** [13].

$$\hat{y} = a + bx \tag{3}$$

where \hat{y} represents the dependent variable, x denotes the independent variable, a is the intercept, and b is the gradient that describes the change in \hat{y} per unit change in x .

3. Result and discussion

3.1 Model validation

Validation is a crucial stage in the numerical modeling of currents and sediment transport. This step plays an essential role in assessing the model's ability to accurately represent the actual physical conditions occurring in the field. The validation process is performed by comparing the model simulation results with observational data, allowing the degree of agreement between the model output and real-world measurements to be evaluated. Through this process, the reliability and accuracy of the model can be assessed, while also identifying potential discrepancies that may arise. The parameter used for validation in this study is tidal water level, comparing the model-generated tide data with observations recorded by the Geospatial Information Agency (BIG) at the Surabaya tide gauge station. The comparison between simulated and observed tidal elevations is presented in **Fig. 3** and **Fig. 4**.

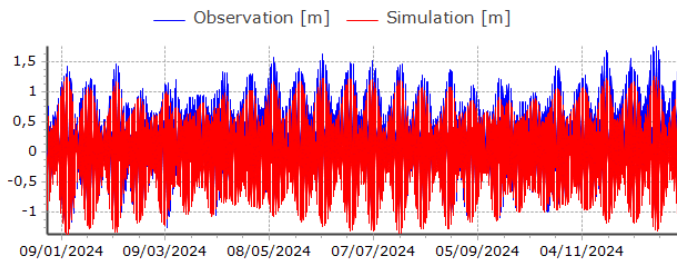


Fig. 3. Comparison of tidal parameters between the model results and BIG observational data.

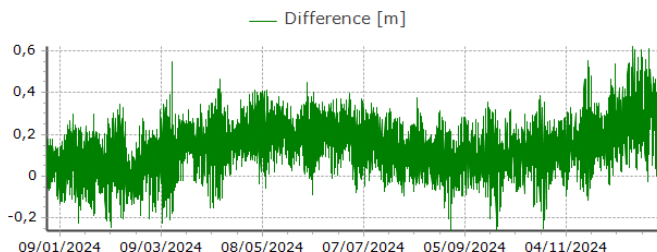


Fig. 4. Differences in tidal elevations between the model results and BIG observational data.

Fig. 3 and **4** sequentially present the tidal elevation plots and the corresponding differences between the model simulation and the BIG observational data from January to December 2024. The largest discrepancy in surface elevation was recorded at 0.62 m on 13 December 2024 at 15:00 UTC. The validation results using the Mean Absolute Error (MAE) and Root Mean Square Error (RMSE) methods are summarized in **Table 4**.

Table 4. Interpretation of MAE and RMSE value

Method	Value
Mean Absolute Error	0.1473 m
Root Mean Square Error	0.1771 m

The statistical evaluation shows that the differences between the two-validation metrics are not significant, indicating that the model errors are relatively uniform and exhibit good predictive stability. Based on the validation results and the classification criteria in **Table 3**, the MAE and RMSE values obtained for each season fall within the *small error* category (< 0.299). Therefore, the model can be considered valid, and the simulation results are suitable for further analysis.

3.2 Current patterns result from the model

The analysis of the hydrodynamic simulation results was carried out under spring tide and neap tide conditions for both the west and east monsoon seasons, with particular focus on the flow characteristics around the Suramadu Bridge piers. This approach was used to identify the maximum current velocities generated under each extreme tidal condition. The determination of spring and neap tide periods for each season was based on the lunar phase

and the modeled tidal elevation data. The simulated tidal curves, along with the identification of spring and neap tide conditions, are presented in **Fig. 5**.

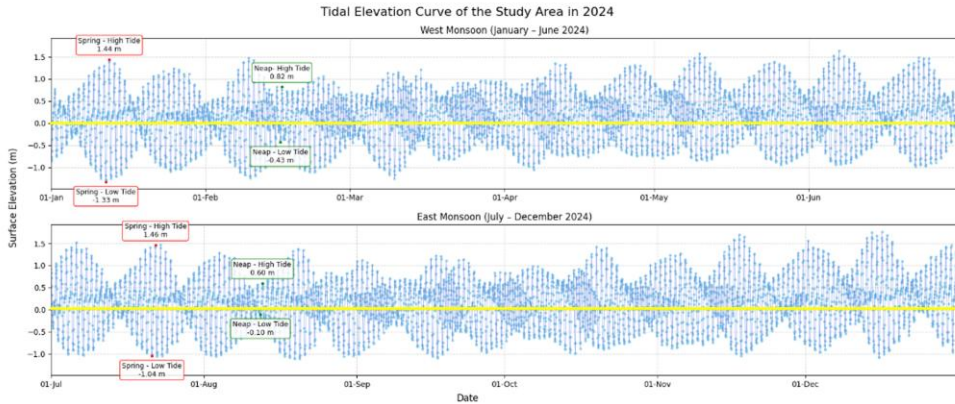


Fig. 5. Tidal elevation graph of the modeled study area in 2024.

Fig. 5 presents the tidal elevation curve for the study area throughout 2024. The blue line illustrates the variability of sea surface elevation, while the yellow line represents the Mean Sea Level (MSL) used as the reference datum. Red markers indicate spring tide conditions, and green markers denote neap tide conditions. During the west monsoon, the spring tide occurred on 12 January 2024, characterized by a minimum water level of -1.33 m at 00:00 UTC and a maximum of 1.44 m at 16:00 UTC on the same day. The neap tide was identified on 16 February 2024, with a minimum elevation of -0.43 m at 01:00 UTC and a maximum of 0.82 m at 08:00 UTC. In the east monsoon, the spring tide occurred on 21 July 2024, marked by a minimum elevation of -1.04 m at 11:00 UTC and a maximum of 1.46 m at 04:00 UTC on 22 July 2024. The neap tide for this season was observed on 12 August 2024, with a minimum level of -0.10 m at 11:00 UTC and a maximum of 0.60 m at 21:00 UTC. These extreme tidal conditions were used as references in determining the simulation scenarios for the hydrodynamic model. By incorporating spring and neap tide conditions from both monsoon seasons, the analysis of current patterns captures both the maximum and minimum energy states associated with tidal forcing, enabling a more comprehensive hydrodynamic assessment.

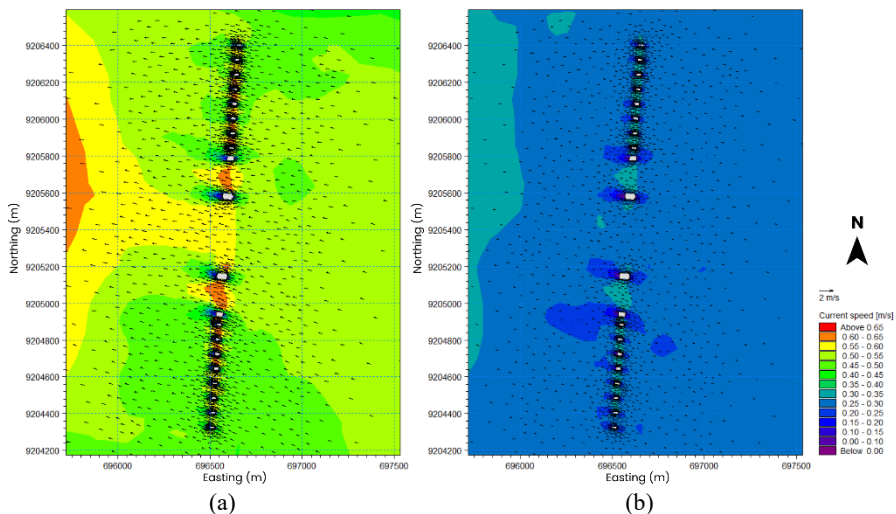


Fig. 6. Current pattern in west monsoon (a) spring tide (b) neap tide.

During the west monsoon, **Fig. 6(a)** shows the distribution of current velocity under extreme spring tide conditions on 12 January 2024 at 05:00 UTC. The currents are predominantly represented by green shades, indicating velocities ranging from 0.40 to 0.55 m/s. The maximum velocities, ranging from 0.60 to 0.65 m/s, are shown in orange and are widely distributed, particularly along the northern and southern sides of the bridge pier structure. In contrast, under the extreme neap tide condition illustrated in **Fig. 6(b)** on 16 February 2024 at 08:00 UTC, the current velocities are generally weaker, dominated by blue shades that represent speeds below 0.30 m/s. The maximum velocities during this neap tide condition fall within the range of 0.30 to 0.35 m/s.

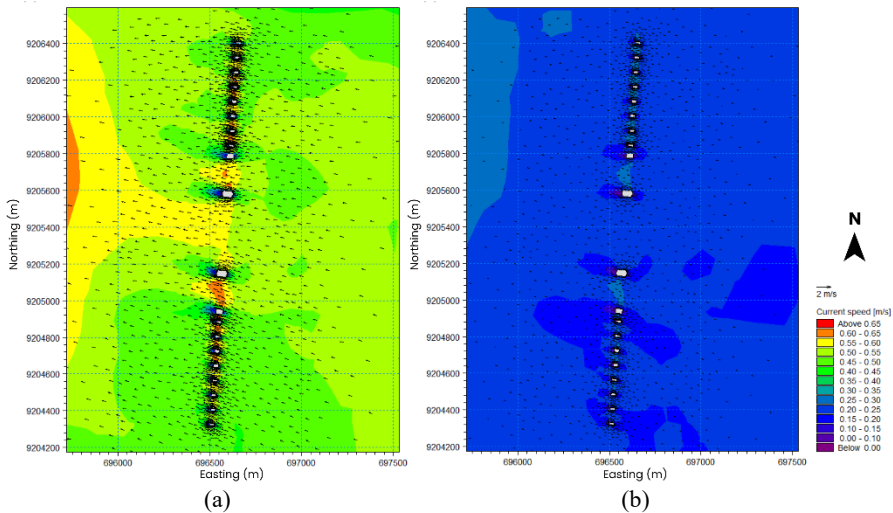


Fig. 7. Current pattern in east monsoon (a) spring tide (b) neap tide.

Meanwhile, during the east monsoon, the distribution of current velocity under extreme spring tide conditions is shown in **Fig. 7(a)** for 21 July 2024 at 16:00 UTC. The current pattern exhibits characteristics similar to those in the west monsoon, with green shades dominating the flow field, indicating velocities between 0.40 and 0.55 m/s. The maximum velocities, ranging from 0.60 to 0.65 m/s, appear along the northern and southern sides of the bridge pier structure. Under the extreme neap tide condition, illustrated in **Fig. 7(b)** on 12 August 2024 at 21:00 UTC, the current velocities are noticeably weaker, dominated by values below 0.25 m/s, with maximum velocities ranging from 0.25 to 0.30 m/s. The bidirectional flow pattern observed in both tidal phases reflects the strong influence of tidal forcing in driving water mass movement in the study area. During flood tide, the generated energy drives the flow westward, while during ebb tide, the flow reverses eastward.

Fig. 8 illustrates the interaction between the current patterns and the P46 bridge pier structure during both monsoon seasons. As described previously, the flow in the study area exhibits a bidirectional pattern, alternating between eastward and westward directions under the dominance of tidal forcing. When the incoming flow encounters the bridge pier, the structure acts as a physical barrier, forcing the water to decelerate. This results in a pronounced reduction in current velocity on the upstream side of the pier both west and east

depending on the flow direction creating a stagnation point, highlighted by the red-circled region.

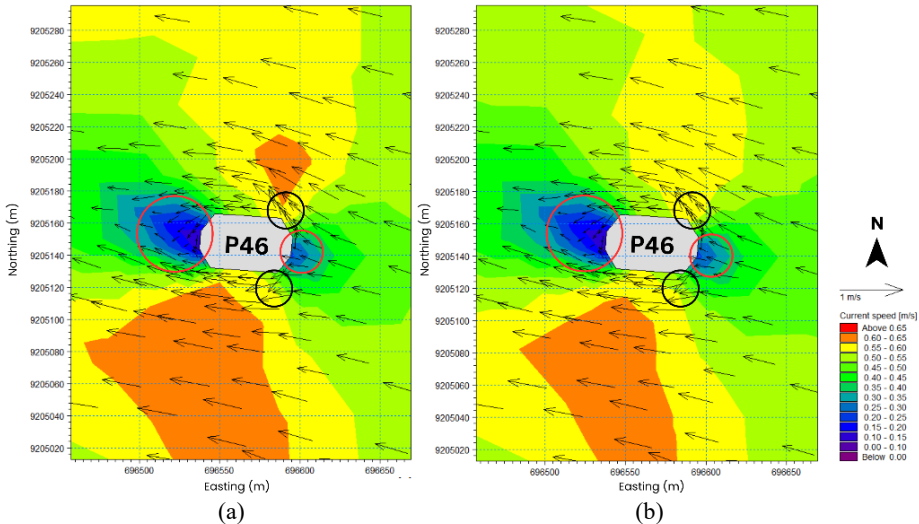


Fig. 8. Interaction between current patterns and bridge piers (a) west monsoon (b) east monsoon.

The presence of the pier also obstructs the natural flow path and constricts the available flow area, causing the water mass to accelerate along the elongated sides of the pier. This flow constriction generates significant velocity amplification along the northern and southern sides, marked by the black-circled region. Once the flow passes the pier, the obstruction is removed and the current gradually returns toward its ambient state; this recovery is evident downstream on the western side of the pier, where the flow begins to spread and velocity decreases toward background levels.

For both monsoon seasons, the reduction in velocity at the stagnation zone ranges from 0.00 to 0.20 m/s, represented by blue to purple shades. Meanwhile, the lateral acceleration around the northern and southern sides reaches 0.50 to 0.65 m/s. Although no major differences are observed between the two seasons in terms of the flow structure interaction mechanism, the west monsoon exhibits a wider distribution of high-velocity zones, particularly north of pier P46.

3.3 Sediment transport result from the model

Sediment transport modeling represents a subsequent stage of the hydrodynamic simulation and aims to understand the dynamics of sediment movement within both the water column and the seabed. The transport process is influenced by interactions among several physical parameters, including current velocity, wave conditions, and sediment characteristics. In this study, sediment transport modeling was conducted to evaluate the potential for both sedimentation and scouring around the bridge piers. The model integrates hydrodynamic outputs with wave conditions and sediment properties as the primary inputs for simulating sediment transport. The sediment characteristics in the vicinity of the Suramadu Bridge piers were classified based on laboratory analyses of sediment samples, as presented in **Table 5**.

Table 5. Laboratory results of sediment sample analysis

Sample Code	Gravel (%)	Sand (%)	Silt + Clay (%)
35 T	0.00	21.49	78.51
29 T	2.55	37.48	59.97
17 T	1.90	94.57	3.53
35 B	1.75	12.22	86.03
29 B	0.00	25.93	74.07
21 B	5.26	88.67	6.07

Based on **Table 5**, the sediment composition is dominated by two major fractions: sand and fine particles (silt + clay). The gravel content is relatively low in all samples, with the highest value recorded at only 5.26% (sample 21 B). Samples such as 17 T (94.57% sand) and 21 B (88.67% sand) are predominantly composed of sand. In contrast, samples 35 T (78.51% silt + clay), 35 B (86.03% silt + clay), 29 B (74.07% silt + clay), and 29 T (59.97% silt + clay) exhibit a dominance of fine sediments.

By combining the sediment fraction characteristics with the seasonal current patterns, the resulting sediment movement around the Suramadu Bridge piers during the west and east monsoons is illustrated in **Fig. 9(a)** and **Fig. 9(b)**.

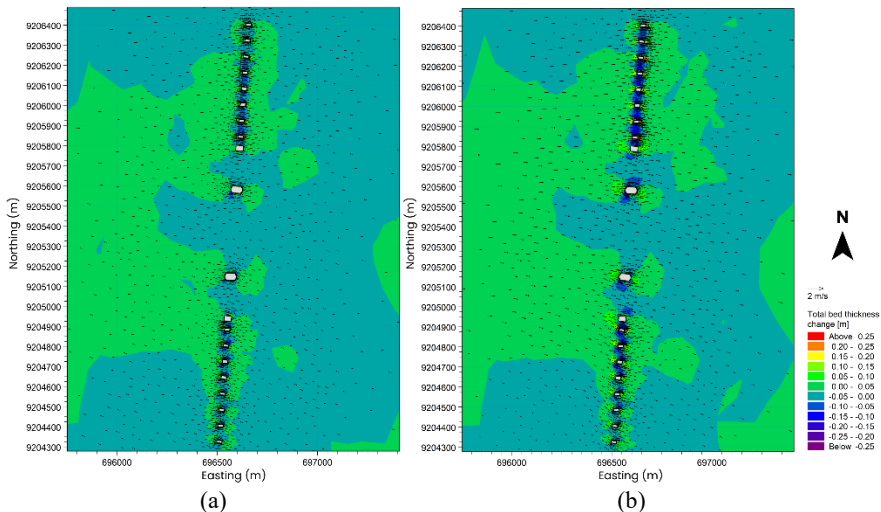


Fig. 9. Sediment transport pattern (a) west monsoon (b) east monsoon.

In both monsoon seasons, the current patterns identified in earlier discussions show that the flow is predominantly driven by tidal forcing, resulting in a bidirectional east–west movement. The interaction between this oscillating flow and the seabed sediment consisting of both cohesive and non-cohesive materials drives the sediment transport processes in the study area. These processes involve the movement of material as bed load and suspended load, producing spatially variable zones of sedimentation and erosion around the Suramadu Bridge piers.

As shown in **Fig. 9(a)**, the cumulative sedimentation erosion pattern during the west monsoon indicates that much of the area around the bridge piers is dominated by erosion, primarily within the range of 0.0 to -0.05 m, while sedimentation mainly occurs within the range of 0.0 to 0.05 m. A similar pattern is observed in the east monsoon, depicted in **Fig. 9(b)**, where erosion remains dominant within the 0.0 to -0.05 m range and sedimentation

remain within the 0.0 to 0.05 m range. Although both seasons exhibit generally similar magnitudes of erosion and sedimentation, differences arise near the pier structures, which will be discussed in the subsequent section. Nonetheless, closer inspection of **Fig. 9(a)** and **Fig. 9(b)** shows that sedimentation becomes more widespread and evenly distributed during the east monsoon compared to the west monsoon, while erosion becomes deeper and expands further around the pier structures. These patterns indicate that sedimentation and erosion processes are continuous between the two monsoon seasons, supported by the similar flow directions and hydrodynamic conditions prevalent throughout the year.

3.4 Bridge pier scour analysis

The reduction in current velocity within the stagnation zone results in a significant decrease in kinetic energy, which in turn lowers the flow's ability to keep sediment particles in suspension or transport them further. In this zone, the current velocity falls below the critical threshold required for sediment entrainment. Consequently, sediment particles lose their carrying force, begin to settle from the water column, and accumulate on the seabed, leading to sedimentation. Conversely, in the lateral zones, the flow is forced to constrict around the pier, resulting in accelerated velocities that increase the kinetic energy and bed shear stress exerted on the seabed. When the applied shear stress exceeds the critical shear stress of the sediment, the bed material becomes mobilized and is carried away by the flow, resulting in erosion.

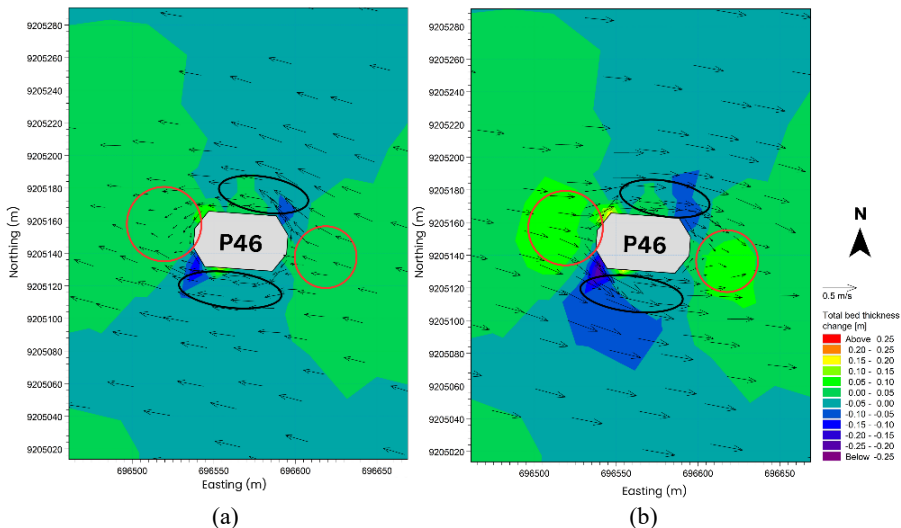


Fig. 10. Sedimentation and erosion patterns around the bridge pier structure (a) west monsoon (b) east monsoon.

During the west monsoon, as shown in **Fig. 10(a)**, erosion occurs along the lateral sides of the pier, reaching values between -0.05 and -0.15 m, while sedimentation on the upstream and downstream sides ranges from 0.0 to 0.05 m. In the east monsoon, the processes of erosion and sedimentation continue, as illustrated in **Fig. 10(b)**. Areas experiencing sedimentation gradually expand over time, and the same applies to zones affected by erosion. This can be observed from the widening extent of both sedimentation and erosion throughout the east monsoon. Sedimentation values around the pier reach 0.05 to 0.10 m, while erosion depths increase to -0.20 to -0.25 m. These conditions indicate that the relatively consistent seasonal flow patterns during both the west and east monsoons produce stable sediment

transport behaviour across the study area and around the pier structure. The recurring seasonal flow directions and magnitudes create persistent zones of potential erosion and deposition. Consequently, despite seasonal variations, the similar hydrodynamic forcing in both monsoons promotes the continuous development of sedimentation and erosion in the same regions over time. This explains why the seabed around the pier exhibits cumulative elevation changes either deposition or scouring throughout the east monsoon.

To identify the pier that experienced the greatest scour depth during the simulation period, the changes in seabed elevation at all bridge piers were compared. The results are presented through the plot in **Fig. 11** and in **Table 6**, which show the maximum scour values at each pier based on elevation changes from the beginning to the end of the 2024 simulation period.

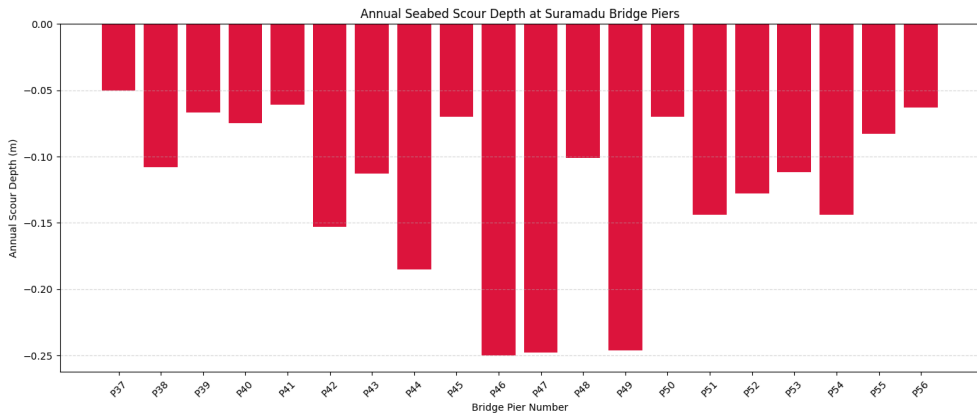


Fig. 11. Comparison of scouring depths at each Suramadu Bridge pier.

Table 6. Comparison of scouring depths at the Suramadu Bridge piers

Piers Number	Scour Depth (m)	Piers Number	Scour Depth (m)
P37	-0.050	P47	-0.248
P38	-0.108	P48	-0.101
P39	-0.067	P49	-0.246
P40	-0.075	P50	-0.070
P41	-0.061	P51	-0.144
P42	-0.153	P52	-0.128
P43	-0.113	P53	-0.112
P44	-0.185	P54	-0.144
P45	-0.070	P55	-0.083
P46	-0.250	P56	-0.063

Based on the table above, pier P46 exhibits the greatest scour depth over the one-year simulation period, with a maximum value of -0.250 m, followed by piers P47 and P49, which recorded scour depths of -0.248 m and -0.246 m, respectively. These piers fall into the category of high-scour structures when compared to the other bridge piers. Pier P37 shows the smallest scour depth at -0.05 m, while other piers with relatively low scour include P41, P56, and P39, each with scour depths less than -0.07 m. As illustrated in **Fig. 11**, the piers that experienced the deepest scour are located near the central section of the bridge, where the water depth is relatively greater. In contrast, the piers with minimal scour are situated in shallower areas. Although not entirely uniform, the results indicate a general tendency:

shallower pier locations exhibit lower scour potential, whereas deeper pier locations are more susceptible to higher scour intensity.

After identifying the piers with the greatest maximum scour depth, the next step is to evaluate the scour rate, which represents the temporal rate of bed degradation around the bridge piers. The scour rate is computed from the slope of the linear regression line fitted to the seabed elevation data for each pier. A more negative regression slope indicates a higher rate of erosion. The regression slopes, and thus the scour rates for each pier, are summarized in **Table 7**.

Table 7. Comparison of scouring rates at the Suramadu Bridge piers

Piers Number	Linear Regression Equation	Regression Slope (Scour Rate)
P37	$y = -0.000138x + 0.002460$	-0.000138
P38	$y = -0.000344x + 0.015517$	-0.000344
P39	$y = -0.000182x + 0.002703$	-0.000182
P40	$y = -0.000214x + 0.006885$	-0.000214
P41	$y = -0.000163x + 0.002825$	-0.000163
P42	$y = -0.000404x - 0.006058$	-0.000404
P43	$y = -0.000298x + 0.001019$	-0.000298
P44	$y = -0.000494x + 0.002646$	-0.000494
P45	$y = -0.000187x + 0.002129$	-0.000187
P46	$y = -0.000641x - 0.023369$	-0.000641
P47	$y = -0.000630x - 0.016320$	-0.000630
P48	$y = -0.000273x - 0.002264$	-0.000273
P49	$y = -0.000626x - 0.032602$	-0.000626
P50	$y = -0.000184x + 0.002551$	-0.000184
P51	$y = -0.000386x + 0.010842$	-0.000386
P52	$y = -0.000339x - 0.003369$	-0.000339
P53	$y = -0.000297x + 0.005101$	-0.000297
P54	$y = -0.000435x + 0.008826$	-0.000435
P55	$y = -0.000217x - 0.001259$	-0.000217
P56	$y = -0.000164x - 0.002892$	-0.000164

Based on the table above, the scour rate for each pier is determined from the slope of its linear regression equation. Pier P46 exhibits the highest scour rate at -0.000641 m/day, followed by piers P47 and P49, with scour rates of -0.000630 m/day and -0.000626 m/day, respectively. These piers fall into the category of high-scour structures when compared to the others. Pier P37 has the lowest scour rate, at -0.000138 m/day, followed by P41 and P56, with scour rates of -0.000163 m/day and -0.000164 m/day, respectively. Taken together both the maximum scour depth and scour rate evaluation piers P46, P47, and P49 represent the structures most significantly affected by scour during the one-year simulation period. The high scour rates at these piers indicate hydrodynamic conditions that promote continuous bed degradation around the pier foundations. Conversely, piers P37, P41, and P56 exhibit relatively stable conditions, characterized by minimal scour depth and low scour rates. Furthermore, the analysis shows that scour locations identified during the west monsoon generally persist into the east monsoon, with consistent erosion patterns observed throughout the one-year simulation. This evaluation serves as an important basis for prioritizing monitoring efforts to ensure the structural integrity of the Suramadu Bridge against long-term scour-related risks.

4. Conclusion

Based on the numerical hydrodynamic modeling conducted in this study, a comprehensive understanding of the current patterns and scour dynamics around the Suramadu Bridge piers has been obtained by incorporating seasonal variability. The flow regime in the study area is predominantly driven by tidal forcing, generating a bidirectional oscillating current with a dominant west–east orientation. Although peak velocities differ between spring and neap tide conditions, the seasonal average current velocities remain relatively stable. Average inflow velocities reached 0.21 m/s on the eastern side of the pier and 0.25 m/s on the western side. The interaction between the incoming flow and the bridge piers produces upstream deceleration and lateral acceleration due to flow constriction. After passing the pier, the flow gradually recovers toward ambient conditions. Velocity reductions of 0.00–0.20 m/s occur at the stagnation zones, while lateral accelerations reach 0.50–0.65 m/s. These hydrodynamic features directly influence the sediment transport processes, generating sedimentation in low-velocity zones and erosion in regions where shear stress exceeds the critical threshold. Sedimentation values range from 0.05 to 0.10 m, while erosion depths reach –0.20 m to –0.25 m.

The one-year simulation further indicates that the most significant scour occurs at piers P46, P47, and P49, with maximum erosion depths of –0.250 m, –0.248 m, and –0.246 m, respectively, accompanied by high scour rates ranging from –0.000641 to –0.000626 m/day. In contrast, piers P37, P41, and P56 exhibit relatively stable conditions, with minimum erosion depths between –0.050 and –0.063 m and low scour rates of –0.000138 to –0.000164 m/day. These results suggest that piers located in shallower waters tend to experience lower scour intensity, whereas deeper-water piers are more susceptible to stronger bed degradation. The scour process is found to be progressive and continuous, as evidenced by consistent erosion patterns across both monsoon seasons. For example, pier P46 experienced –0.075 m of scour during the west monsoon and –0.175 m during the east monsoon, resulting in a cumulative erosion depth of –0.250 m by the end of the simulation. The persistence of negative scour rates throughout the year indicates that the seasonal flow regime plays a major role in maintaining stable and progressive scour zones around the pier foundations over time.

Acknowledgement

The authors gratefully acknowledge financial support from the Institut Teknologi Sepuluh Nopember for this work, under project scheme of the Publication Writing and IPR Incentive Program (PPHKI) 2025. The authors further acknowledge PT. Hidronav Teknikatama, PT. Geosolution Pratama Nusantara and the Hydro Fieldcamp and Hydrography 2024 team for their assistance in the data collection process for this study.

References

- [1] Presiden Republik Indonesia, Keputusan Presiden (Keppres) Nomor 55 Tahun 1990 tentang Pembangunan Jembatan Surabaya–Madura, Pemerintah Pusat (1990). <https://peraturan.bpk.go.id/Details/63993/keppres-no-55-tahun-1990>
- [2] M. Effendi, Dampak Pembangunan Jembatan Suramadu Terhadap Perekonomian Pulau Madura (Studi Kasus Kabupaten Bangkalan), Universitas Diponegoro (2013). <http://eprints.undip.ac.id/42107/>

- [3] I.A. Dumatubun, W.S. Pranowo, A. Sartimbul, J. Setiyadi, S.H. Sari, F.O. Setyawan, Karakteristik arus permukaan laut pada selatan Madura. *J. Chart Datum* **10**, 1 (2024)
- [4] A. Siswanto, Sebaran Total Suspended Solid (TSS) pada profil vertikal di perairan Selat Madura Kabupaten Bangkalan. *J. Kelautan* **8**, 26–32 (2015).
- [5] Chomaedhi, Pelaksanaan pondasi bored pile 240 cm Main Bridge – Jembatan Suramadu. Seminar Nasional Aplikasi Teknologi Prasarana Perkotaan, Surabaya (2008).
- [6] A. Dictanata, L. Lutjito, Pengaruh penempatan tirai satu baris pada pilar jembatan terhadap kedalaman gerusan. *J. Tek. Sipil Arsitektur* **12**, 2 (2016). <https://doi.org/10.21831/inersia.v12i2.12587>
- [7] H. Armono, A. Budipriyanto, Study on local scouring at Suramadu Bridge piers for structural integrity monitoring. *Proc. 7th Int. Conf. Asian and Pacific Coasts (APAC)*, Bali, 107–112 (2013).
- [8] F.H. Putra, D.G. Pratomo, Analisis arus dan transpor sedimen menggunakan pemodelan hidrodinamika 3 dimensi (Studi kasus: Teluk Ambon, Kota Ambon, Maluku). *J. Tek. ITS* **8**, 2 (2019).
- [9] Consortium of Chinese Contractors, Detailed Design of Main Bridge for Indonesian Suramadu Bridge Project, (2005).
- [10] H. Hersbach, B. Bell, P. Berrisford, G. Biavati, A. Horányi, J.M. Sabater, J. Nicolas, ERA5 hourly data on single levels from 1940 to present. *C3S Climate Data Store* (2023). <https://doi.org/10.24381/cds.adbb2d47>
- [11] U. Lasminto, Studi potensi tampungan air sebagai sumber air baku Kota Surabaya. *Simposium I Jaringan Perguruan Tinggi untuk Pembangunan Infrastruktur Indonesia* (2016), No. 5 (2017). <https://doi.org/10.12962/J23546026.Y2017I5.3113>
- [12] M.K. Khotimah, Validasi Tinggi Gelombang Signifikan Model Gelombang Windwave-5 Dengan Menggunakan Hasil Pengamatan Satelit Altimetri Multimisi, Universitas Indonesia (2022).
- [13] N. Roustaei, Application and interpretation of linear regression. *Med. Hypothesis Discov. Innov. Ophthalmol.* **13**, 3, 151–159 (2024). <https://doi.org/10.51329/mehdiophthal1506>